Experimental investigation of wing tip vortices in the near-field

Robert Stepanov[1*], *Vladimir* Pakhov[1], *Andrey* Bozhenko[1], *Alexander* Kusyumov[1], *Sergey* Mikhailov[1] and *Nikolay* Tarasov[2]

[1]Kazan National Research Technical University named after A.N. Tupolev, Department of Aerohydrodynamics, 420111, 10 Karl Marx Street, Kazan, Russian Federation.
[2]The Central Aerohydrodynamic Institute (TSAGI), 140180, 1 Zhukovsky Street, Zhukovsky, Russian Federation.

Abstract. Results of an experimental investigation related to near-field wing tip vortices are presented. The measurements were carried out using a PIV-system in T-1K wind tunnel of KNRTU-KAI. Q-criterion and cross-sectional lines method were used to determine vortex core locations, which showed a good agreement. It is shown that the circulation of tip vortices remains constant at low to moderate angles of attack, and decreases in the stream-wise direction for higher angles of attack. It is also shown that the vortex core radius increases in the stream-wise direction, taking larger values at higher angles of attack.

1 Introduction

Stream-wise vortices are encountered in a wide range of practical applications. These vortices are known to be intense and persistent and cause many adverse effects in different practical applications, especially in finite span wings and rotary wings. This includes high acoustic noise, vibrations and mechanical fatigue [1].

The wake vortices generated by large aircraft pose danger to following aircraft, especially during landing and take-off [2], which limits the capacity of airports [3,4]. Therefore, the dynamics of wing tip vortices after roll-up and until their decay is an important subject which has been studied by many researchers [5,6].

Some of the recent experimental investigations include the work of Sun and Daichin [7], where the influence of the ground effect on the wing tip vortices was investigated on a NACA0012 wing. Ahmadi-Baloutaki et al. [8] carried out experiments on the effect of the external free-stream turbulence in the near-field of a wing-tip vortex using hot-wire anemometry, which showed that the increase of the external free-stream turbulence tends to increase the vortex diffusion.

Up to date, many physical aspects of the vortex formation and evolution are not well understood. This work was aimed at investigating near-field wing tip vortices in wind tunnel conditions.

* Corresponding author: rpstepanov@kai.ru

2 Experimental setup

The experimental results were obtained at KNRTU-KAI in T-1K wind tunnel, which is a low speed, closed-circuit and open-jet wind tunnel with a contraction ratio of 4.9 [9]. The T-1K wind tunnel has a free-stream turbulence intensity levels below 0.5% in the jet core and a nozzle exit diameter of 2.25 m.

Experiments were carried out on a rectangular wing, having an aspect ratio of *AR*=7.8 and the chord length b=187 mm. The wing had a cross section of a modified Göttingen 387 aerofoil, which had a flat lower surface compared to the original aerofoil. The wind speed was set to V_∞=28 m/s, which corresponded to a Reynolds number *Re* = 350 000. The modified Göttingen 387 aerofoil was chosen in part because it was previously used in an experimental study of a new wind turbine concept [10].

Velocity fields were obtained using Dantec PIV system with *Nd-YaG laser Litron 425-10*, having the maximum power output of 425 mJ, exposure time 6 ns and the wave length of 532 nm. Exposure frequency corresponded to 8 Hz. The flow was seeded with olive oil particles using a liquid seeding generator 10F03. The olive oil was chosen due to its good time response in a decelerating flow [11].

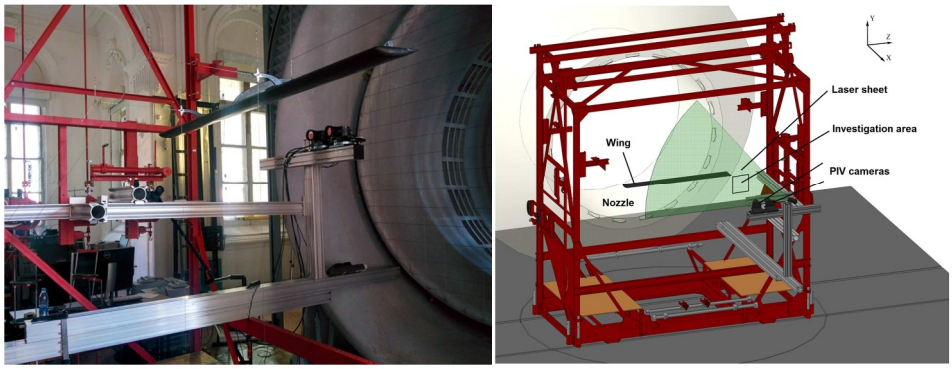

(a) (b)

Fig. 1. Experimental setup at T-1K wind tunnel: (a) photo of the experimental setup and (b) 3D model of the experimental setup.

The experimental setup is shown in Figures 1(a) and 1(b). The PIV camera *FlowSenseEO 4M*, with the resolution of 2048×2048 pixels, was positioned behind the wing in order to capture the wing tip vortex, as shown in Figure 1(b). The distance between the laser sheet and the camera did not change during the experiments. The directions of axes *X*, *Y* and *Z* are defined in Figure 1(b). Tip vortices were measured at different distances *x* from the trailing edge of the wing to the laser sheet ($10 \leq x \leq 790$ mm). Measurements were performed for a wide range of angles of attack (α=−6°, 0°, 6°, 12° and 18°) in order to capture the range from the zero lift coefficient to maximum lift coefficient.

Adaptive PIV algorithm was used to obtain velocity fields from the raw camera images. Due to significant centrifugal forces exerted on the seed particles inside the vortex, they tend to spiral radially outward. This creates areas with low density of seed particles, which requires increasing the grid size during the data processing in order to successfully identify velocity vectors within the viscous core of the vortex. This was achieved by setting the grid step size and the minimum interrogation area size to 4 mm.

3 Vortex identification

3.1 *Q*-criterion

Q-criterion defines vortices as connected spatial regions, where the Euclidian norm of vorticity tensor $\boldsymbol{\Omega}$ is larger than the rate of strain tensor $\boldsymbol{S}$ [12]:

$$Q = 0.5[|\boldsymbol{\Omega}|^2 - |\boldsymbol{S}|^2] > 0. \quad (1)$$

Due to the fact that in this work obtained data corresponded to 2D velocity fields, $\boldsymbol{\Omega}$ and $\boldsymbol{S}$ values were reduced to a 2D form:

$$|\boldsymbol{\Omega}|^2 = (\partial u/\partial y - \partial v/\partial \mathrm{x})^2, \quad (2)$$

$$|\boldsymbol{S}|^2 = 2(\partial u/\partial x)^2 + 2(\partial v/\partial y)^2 + (\partial u/\partial y + \partial v/\partial x)^2. \quad (3)$$

The size of each vortex was obtatined from the condition $Q > 0$. Due to large amount of experimental data, Q-criterion was applied only to statistically averaged velocity fields. The size of every vortex is presented in terms of a relative radius r_{eq}:

$$r_{eq} = (F/\pi)^{0.5}/\mathrm{b}, \quad (4)$$

where b is the chord of the wing, and F is the vortex area obtained from the condition $Q>0$.

The circulation was calculated along outside boundaries C of the vortex, defined by the condition $Q>0$:

$$\Gamma = -\oint \mathbf{V}\cdot\mathbf{dl}. \quad (5)$$

3.2 Cross-sectional lines (CSL) method

The cross-sectional lines algorithm [13] has been used for obtaining coordinates of the tip vortices. In this method, a vortex origin is defined as a point, where the differences of largest and smallest tangential components of velocities along horizontal and vertical axes take largest values. To this end, a code was written to find vortex coordinates for each distance from the trailing edge to the laser sheet and for every angle of attack.

4 Results and discussion

While streamlines can be used to locate a vortex, difficulties can emerge in the vicinity of the vortex due to low density of tracer particles within the viscous core. In Figure 3(a) a raw camera output is shown. A low tracer particle density area corresponds to the position of the viscous core of the vortex. However, it can only be used as an estimate of the vortex position and its size, due to no clear boundary separation of the sparsely seeded region from normally seeded regions. Instead, the density of seeded particles gradually decrease towards the vortex center.

A sample velocity field from PIV measurements, is shown in Figure 3. The angle of attack α=18° was chosen because vortex assymetry becomes more pronounced at higher angles of attack.

CSL-method has been used to obtain the vortex origin position. The distribution of tangential components (V_y and V_z) along Y and Z axes, passing through the vortex origin, were then obtained and are shown by white lines in Figure 3(a) and black lines in Figure 3(b). V_y and V_z were non-dimensionalized relative to the free-stream velocity V_∞. The

vortex core is confined within the peak tangential velocities V_y and V_z, which are indicated by dashed lines in Figure 3(b). The vertical and horizontal distances (y and z) were nondimensionalized with respect to the wing chord b.

The vortex wandering was estimated from vortex coordinates obtained using the CSL-method from an ensemble of 30 velocity fields for each measurement case. The root-mean-sqaure devation from the average vortex position changed from 1.2% of the wing chord length in the vicinity of the trailing edge, to 5% at fartherst stream-wise distance.

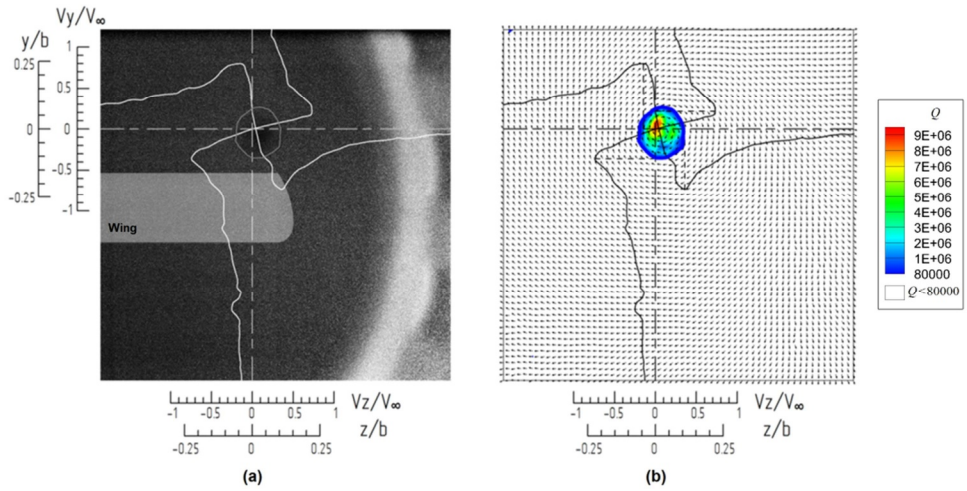

Fig. 3. Locating vortex core using CSL and Q-criterion methods: (a) a raw camera output with tracer particles; (b) velocity field and vortex position obtained from Q-criterion. The distance from the trailing x/b =3.209 and the angle of attack α=18°.

The vortex core obtained from Q-criterion is depicted in Figure 3(b). Here, only the region, satisfying the condition Q>80000, is shown for clarity to eliminate small descrete regions of vorticity in the vicinity of the vortex core. As can be seen from Figure 3(b), the vortex origin obtained from CSL-method corresponds to the maximum value of Q. However, the vortex core origin is displaced from the geometric center, which is sometimes used for preliminary vortex identification from low density areas of the seeded tracer particles. A similar analysis for other angles of attack and different distances from the trailing edge has shown that vortex position obtained using CSL-method correspond to maximum value of Q, and that low density of seeded tracer particles can be used only as an estimate of the vortex origin.

The variation of the vortex core radius r_{eq} with stream-wise distance x/b is plotted in Figure 4(a) for different angles of attack. As can be seen, vortices tend to increase in size downstream of the wing and for increasing angles of attack. The vortex core radius r_{eq} growth rate is similar for higher angles of attack (α=12° and α=18°).

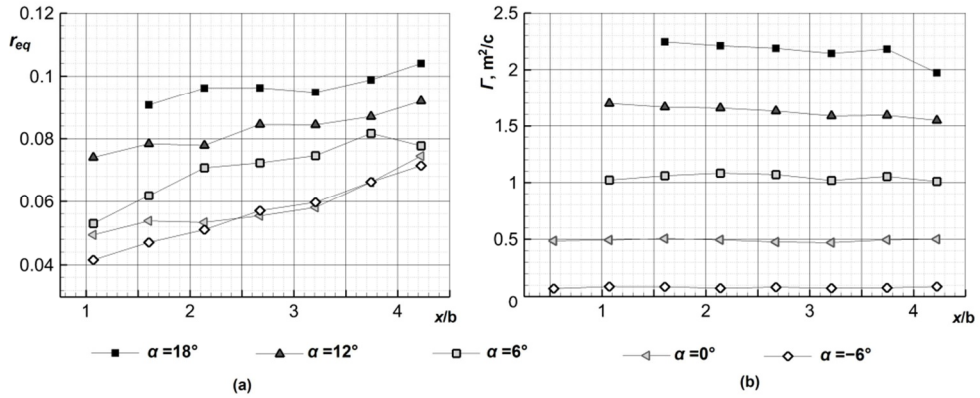

Fig. 4. Characteristics of the wing tip vortices for different distances *x*/b from the trailing edge: (a) equivalent vortex radii and (b) circulation distribution.

Figure 4(b) shows circulation distribution Γ with the stream-wise distance *x*/b for different angles of attack. There is a linear dependency of circulation. As can be seen, circulation does not change at lower angles of attack (α=−6°, α=0° and α=6°). However, at higher angles of attack (α=12°, α=18°), a steady linear decline of circulation is observed for the increasing stream-wise distance *x*/b. It should also be noted that a linear dependency can be observed of the circulation Γ distribution with respect to the stream-wise distance *x*/b. The circulation takes very low values at α=−6°, due to being close to the angle of zero lift coefficient.

5 Conclusions

In this work experimental results of the wing tip vortices, obtained using Dantec PIV system, have been presented. The measurements of the tip vortices were taken at different stream-wise directions, ranging from 0.5 to 4.2 chord distances, and for different angles of attack.

The comparison of the Cross-Sectional Line algorithm and Q-criterion showed good agreement in the identification of the vortex core positions.

The dependence of the vortex core radius with respect to the stream-wise distance has been presented for different angles of attack. It was shown that the vortex areas tend to increase in size in the stream-wise direction. The vortex core size increases for higher angles of attack.

The circulation distribution of the tip vortices for low and moderate angles of attack ($-6° \le \alpha \le 6°$) remains constant in the stream-wise direction. However, there is a steady decline of the circulation in the stream-wise direction for higher angles of attack (α=12° and α=18°). It is shown that the circulation exhibits a linear dependence on the stream-wise distance from the wing to the tip vortex location.

This work was supported by the grant ‘Numerical and physical modelling of aerodynamic and aeroacoustic characteristics of rotor systems of future concept aircarft’ (No. 9.1577.2017/4.6) of the Ministry of Education and Science of the Russian Federation.

References

1. A.L. Heyes, D.A.R. Smith, Aerosp Sci Technol **9,** 469–475 (2005).
2. F. Holzäpfel, J. Kladetzke, J. Aircr., **48**, 812–822 (2011).
3. J.N. Hallock, G.C. Greene, D.C. Burnham, Air Traffic Control Quarterly **6**, 161–178 (1998).
4. T. Gerz, F. Holzäpfel, D. Darracq, Prog. Aerosp. Sci. **38**, 181–208 (2002).
5. P.R. Spalart, Annu. Rev. Fluid Mech. **30**, 107–138 (1998).
6. V. Rossow, Prog. Aerosp. Sci. **35**, 507–660 (1999).
7. R. Sun, Daichin, Theor. Appl. Mech. Lett. **1**, 032001-1–032001-6 (2011).
8. M. Ahmadi-Baloutaki, R. Carriveau, D.S.-K. Ting, Aerosp Sci Technol **43 ,** 395–405 (2015).
9. V.V. Zherekhov, V.V. Pakhov, Proceedings of the 10th International Chatayev Conference **1**, 161–168 (2012, in Russian).
10. M. Valiev, R. Stepanov, V. Salakhov, V. Zherekhov, G.N. Barakos, Aeronautical Journal **118**, 1229-1224, 2014.
11. M. Raffel, C.E. Willert, S.T. Wereley, J. Kompenhans, *Particle Image Velocimetry: A Practical Guide*, 15-18 (2017).
12. G. Haller, J. Fluid Mech. **525,** 1199-1207 (2005).
13. H. Vollmers, Meas Sci Technol **12**, 1199-1207 (2001).